Nanoscale

Accepted Manuscript

This is an *Accepted Manuscript*, which has been through the RSC Publishing peer review process and has been accepted for publication.

Accepted Manuscripts are published online shortly after acceptance, which is prior to technical editing, formatting and proof reading. This free service from RSC Publishing allows authors to make their results available to the community, in citable form, before publication of the edited article. This *Accepted Manuscript* will be replaced by the edited and formatted *Advance Article* as soon as this is available.

To cite this manuscript please use its permanent Digital Object Identifier (DOI®), which is identical for all formats of publication.

More information about *Accepted Manuscripts* can be found in the **Information for Authors**.

Please note that technical editing may introduce minor changes to the text and/or graphics contained in the manuscript submitted by the author(s) which may alter content, and that the standard **Terms & Conditions** and the **ethical guidelines** that apply to the journal are still applicable. In no event shall the RSC be held responsible for any errors or omissions in these *Accepted Manuscript* manuscripts or any consequences arising from the use of any information contained in them.

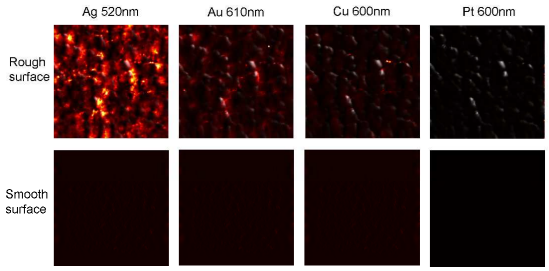

A photovoltaic enhancement is due to surface-plasmon assisted visible-light absorption at the inartificial surface of PZT film.

Photovoltaic Enhancement Due to Surface-Plasmon Assisted Visible-Light Absorption at the Inartificial Surface of Lead Zirconate-Titanate Film

Fengang Zheng,[a,b,*] Peng Zhang,[a] Xiaofeng Wang,[a] Wen Huang,[b,c] Jinxing Zhang,[d,e] Mingrong Shen,[a] Wen Dong,[a] Liang Fang,[a] Yongbin Bai,[f] Xiaoqing Shen,[f] Hua Sun[a,*] Jianhua Hao,[b*]

[a]*Department of Physics and Jiangsu Key Laboratory of Thin Films, Soochow University, Suzhou 215006, China*

[b]*Department of Applied Physics, Hong Kong Polytechnic University, Hong Kong, China*

[c]*State Key Laboratory of Electronic Thin Films and Integrated Devices, University of Electronics Science and Technology of China, Chengdu, 610054, China*

[d]*Department of Physics, Beijing Normal University, Beijing, 100875, China*

[e]*Key Laboratory of Theoretical and Computational Photochemistry, Ministry of Education, Beijing Normal University, Beijing, 100875, China*

[f]*China Satellite Maritime Tracking and Controlling Department, Jiangyin 214431, China*

Abstract:

PZT film of 300 nm thickness was deposited on the tin indium oxide (ITO) coated quartz by sol-gel method. Four metal electrodes, such as Pt, Au, Cu and Ag, were used as top electrodes deposited on the same PZT film by sputtering at room temperature. In ITO/PZT/Ag and ITO/PZT/Au structures, the visible light (400-700 nm) can be absorbed partially by PZT film, and the maximum efficiency of

photoelectric conversion of ITO/PZT/Ag structure was enhanced to 0.42% (100 mW/cm^2, AM 1.5G), which is about 15 times higher than that of ITO/PZT/Pt structure. Numerical simulations show the natural random roughness of polycrystalline-PZT/metal interface can offer a possibility of the coupling between the incident photons and SPs at the metal surface. The coincidence between the calculated SP properties and the measured EQE spectra reveals the SP origin of the photovoltaic enhancement in these ITO/PZT/metal structures, and the improved photocurrent output is caused by the enhanced optical absorption in the PZT region near the metal surface, rather than by the direct charge-transfer process between two materials.

Keywords: Ferroelectric film; Photovoltaic; Surface plasmons; Metal work function

1. Introduction

Recently, photovoltaic effects of the ferroelectric films, such as $Pb(Zr,Ti)O_3$ (PZT, including $PbTiO_3$ and $(Pb,La)(Zr,Ti)O_3$),[1–6] $BiFeO_3$ (BFO),[7–13] $(Bi,Nd)Ti_3O_{12}$[14,15] and Bi_2FeCrO_6,[16] are currently receiving a great deal of interest as a promising alternative to conventional photonic and photovoltaic devices. Attention has been focused on the influence of interface effects,[17-22] crystal orientation,[23] domain wall,[9,24] and grain boundaries or defects.[25-28] The photovoltaic effect of ferroelectric films shows an impressive characteristic and potential application prospect such as a huge open-circuit voltage (V_{OC}) 15V.[9,24] However, the main drawback of this intriguing effect is that only a tiny short-circuit photocurrent (J_{SC}) is generated because these highly-insulating ferroelectric materials have a typical large band gap, for example, PZT is about 3.6 eV that can only absorb the ultraviolet light (UV) with the wavelength from 300 to 380nm.[29] Although the band gap of BFO is about 2.7 eV that is lower than that of PZT, BFO can only absorb the light with the wavelength below 450 nm.[17] In our recent works, some semiconductors with narrow band gap such as Cu_2O (2.7 eV)[29] and Ag_2O (1.2 eV)[30] were introduced into PZT film to form new type solar cell, which just show a weak absorption of visible light. In these works, the short-circuit current (J_{SC}) of PZT film was enhanced greatly at the cost of remnant polarization, which was indicated by the decrease of the open-circuit voltage (V_{OC}).

Many studies[4,15,18,29] of photovoltaic mechanism in the electrode/PZT/electrode structures have revealed that the photocurrent is determined mainly by the bottom Schottky barrier ($E_{bi\text{-}bottom}$) at the interface between the bottom electrode and PZT film

because the value of top Schottky barrier ($E_{bi\text{-}top}$) is far lower than that of $E_{bi\text{-}bottom}$ and this two Schottky barriers are back-to-back, as shown in Fig. 1a. Since the direction of the $E_{bi\text{-}bottom}$ is pointed to the bottom tin indium oxide (ITO) electrode, the UV light-induced holes (h_{BB}) are expelled to the bottom ITO electrode and the UV light-induced electrons (e_{BB}) are drifted to the top metal one.[29] Most of e_{BB}s at the top interface will be expelled back to the PZT film due to the existing of the $E_{bi\text{-}top}$, which limits the photocurrent of PZT film. The works of Harshan[2] and Su[31] show that the top electrodes with a low work function, such as Al (4.2 eV) or Mg (3.7 eV), can enhance effectively the photovoltaic output of the metal/ferroelectric/metal structures, which is attributed to the reduction of Schottky barrier height at top metal/ferroelectric interface. However, these improvement of photovoltaic output are still restricted to enhancing the band-to-band absorption (UV light) of PZT film.

Surface plasmon (SP) structures (mainly Ag or Au nanoparticles incorporated in or on semiconductors) can improve the photovoltaic performance of solar cells in the visible range, which has been verified by many previous works.[32] SP refers to the collective excitation of conduction electrons at a metal/dielectric interface. The associated electromagnetic field distributions in the vicinity of the interface will exhibit strong confinement and enhancement, as well as sensitivity to the geometry of the metallodielectric structures and the optical constants of the materials. For thin film solar cells based on semiconductors with a narrow band gap, such as Si, GaAs and CdSe/Si heterostructures,[33,34] researchers usually adopted properly engineered SPs to couple and trap the incident light into the semiconductor film and enhance optical

absorption, which leads to the increased production rate of the electron-hole pairs, particularly in the near-field region of the semiconductor/metal interface. Usually, SP can performance efficiently only at an artificial periodic metal structure[35] or a well-designed nanoparticle metal/semiconductor interface,[33,34] which undoubtedly increases the technical complexity and the process cost.

For solar cells based on the PZT film with a band gap of about 3.5 eV, no studies of their photovoltaic performance with SPs have been reported, at least to our knowledge. But both experiment and analytic calculation have shown that SPs in the visible band will occur when Au nanoparticles are embedded in the PZT matrix[36] or when periodic Au structures are introduced,[35] just like what happens when these nanostructured metals are incorporated into other semiconductors. In this paper, we report a new mechanism in a simple structure that can improve the visible-light absorption of PZT film, as shown in Fig. 1b. The PZT film of 300 nm thickness was deposited on the ITO (150nm, Supporting Information Fig. S1, and the detailed experimental process can be found elsewhere.[29]) coated quartz by sol-gel method. Ag was deposited on the PZT film by sputtering at room temperature as top electrode with a low work function (4.26 eV) that is close to that of Al metal and leads to a low $E_{bi\text{-}top}$ (To simplification, $E_{bi\text{-}top}$ is neglected in Figur 1b). Meanwihle, Ag has been extensively investigated as one of good candidates for SP applications in the visible range due to its low loss and high stability.[32] The visible-light induced charges (h_{SP} and e_{SP}) can also be separated efficiently by the $E_{bi\text{-}bottom}$ if the $E_{bi\text{-}top}$ is as low as possible. In ITO/PZT/Ag structure, the visible light (400-550 nm) can be absorbed

partially by PZT film, and the maximum efficiency of photoelectric conversion was enhanced to 0.42% (100 mW/cm^2, AM 1.5G), which is about 15 times higher than that of ITO/PZT/Pt structure. Au is another candidate for SP application, which has a high work function (5.1 eV).[35] Copper (Cu, work function 4.56 eV) exhibits an SP resonance similar to that of Au in numerical simulations, but easily suppressed by oxidation in experiments.[37,38] Platinum (Pt) with a highest work function (5.6 eV) is among the poor material to support SP due to is heavy damping.[39] In our experiments, Pt, Au and Cu metal electrodes were deposited on the same PZT film at room temperature for the comparative studies. Note that no artificial nanostructures such as metallic nanoparticles or periodic metallic structures are introduced deliberately in our experiments. However, it is interesting that our calculations will show the natural random roughness of polycrystalline-PZT/metal interface can also offer a possibility of the coupling between the incident photons and SPs at the metal surface.

2. Experimental

PZT films were deposited by sol-gel method. The experimental details can be found in our previous works.[29] Metal Pt, Au, Cu and Ag dots (Diameter and thickness of these dot electrodes were about 300 μm and 80 nm, respectively) as top electrodes were fabricated on the same PZT film by sputtering at room temperature. Polarization-voltage (P-V) hysteresis loops were examined using a precision ferroelectric analyzer from Radiant Technology. Current density-voltage (J-V) characteristics of PZT film with Pt, Au, Cu and Ag top electrodes were recorded by 91160 of Newport under a simulated sunlight (AM1.5G, 100 mW/cm^2).

Time-dependent open-circuit voltage (V_{OC}) and short-circuit current (J_{SC}) under the illumination of the incident light with various wavelengths were recorded by Keithey 6517 A. The surface morphologies of the film was investigated using a NTMDT Solver P47-PRO scanning probe microscope operating in the contact atomic force microscope (AFM) mode. EQE (external quantum efficiency) was measured by IPCE/QE 200 of Newport within the wavelength of 300-750 nm. UV-visible light transmission and absorption characteristic were measured by JASCO UV/VIS 550.

3. Results and discussion

Fig. 2 shows the polarization hysteresis loops of ITO/PZT/Pt, ITO/PZT/Au, ITO/PZT/Cu and ITO/PZT/Ag structures. Because four types top electrodes were deposited on the same PZT film, as shown in the inset of Fig. 2, all structures have the same saturation polarization. However, the remnant polarization ($2P_r$) of ITO/PZT/Pt, ITO/PZT/Au, ITO/PZT/Cu and ITO/PZT/Ag structures is 54.6, 51.8, 48.0 and 42.3 $\mu C/cm^2$, respectively, influenced by the work function of top electrodes. Among four top electrodes, only the work function (4.26 eV) of Ag electrode is far lower than that (4.6 eV[29]) of PZT film, so, more injected charges may be introduced into the PZT film when a poling voltage was applied on ITO/PZT/Ag sample. The $2P_r$ of ITO/PZT/Ag is lower a little than those of other three structures, which is mainly attributed to more injected charges in ITO/PZT/Ag structure due to the low work function of Ag electrode, as a result, partially polarization trapping.[40,41]

The photovoltaic output of ITO/PZT/metal structure is mainly determined by the bottom Schottky barrier of ITO/PZT interface ($E_{bi\text{-}bottom}$) and modulated by the

polarization switching (Supporting Information Fig. S2).[29,42] When the PZT film is remnant polarization-up state, the direction of the depolarization field due to the aliment polarization is the same as that of the $E_{bi\text{-}bottom}$, so, a maximum photovoltaic output can be obtained. Fig. 3 displays the representative current density-voltage (J-V) characteristic of ITO/PZT/Pt, ITO/PZT/Au, ITO/PZT/Cu and ITO/PZT/Ag structures, respectively, recorded under AM 1.5G (100 mW/cm^2) illumination when PZT film is remnant polarization-up state. The open circuit voltage (V_{OC}), short circuit current (J_{SC}), fill factor (FF) and photoelectric transformation efficiency (η) of all structures are listed in Supporting Information Table S1. Except the ITO/PZT/Ag structure, the V_{OC} increases with the decrease of the work function of metal electrode, which can be attributed to the decrease of the top Schottky barrier height,[2,31] considering these three samples have a similar $E_{bi\text{-}bottom}$ and remnant polarization. The V_{OC} of ITO/PZT/Ag structure is lower a little than that of ITO/PZT/Cu structure, which is due to the decrease of the remnant polarization of ITO/PZT/Ag structure. It is interesting that the ITO/PZT/Ag structure has the largest J_{SC} among those of four structures. Harshan[2] reported that by using aluminum, a low work function metal (4.2 eV), as top electrode, the photocurrent magnitude can be enhanced about 3 times higher than that using Pt as top electrode in La doped PZT film. However, the work function of Ag (4.26 eV) is comparable to that of Al, the J_{SC} of ITO/PZT/Ag structure is about 12 times than that of ITO/PZT/Pt structure. Furthermore, the J_{SC} of ITO/PZT/Au structure are about 2 times higher than that of ITO/PZT/Cu while the work function of Au is higher than that of Cu. Obviously, the J_{SC} is not linearly dependent of the work function of top

metal electrode, which cannot be explained only by the decrease of the work function of top electrode.

We tried to add different filters between the sample and the simulated sunlight source in order to change the wavelength and the power of incident light. The filters were named by K9, JB420 and CB550, respectively, and the transmission spectra of these filters can be found in Supporting Information Fig. S3. The absorption wavelength edges of K9, JB420 and CB550 are 285, 400 and 555 nm, respectively and the powers of transmitted lights were 95, 86 and 40 mW/cm^2, respectively. Fig. 4 shows time-dependent J_{SC} of four structures illuminated under the incident light with different wavelength and power. It seems reasonable that the J_{SC} decreases with the incident light power, as shown in Fig. 4. When the incident light includes only the visible light (JB420 and CB550 filters), it is easy understandable that the J_{SC} is close to zero in both ITO/PZT/Pt and ITO/PZT/Cu structures, as shown in Fig. 4a and 4c, because the band gap of PZT is about 3.6 eV, which is almost transparent for visible light. However, in the ITO/PZT/Ag structure, a J_{SC} (about 0.7 mA/cm^2) can be observed when the sample is lighted only under the visible light (>400 nm), as shown in Fig. 4d. Furthermore, in the ITO/PZT/Au structure as shown in Fig. 4b, a steady J_{SC} is still obtained when the wavelength of incident visible light is longer than 550 nm. Pintilie[19] and Takahashi[43] have reported a sub-bandgap absorption in epitaxial PZT or $PbTiO_3$ films, which can result in a very tiny visible light-induced photocurrent. Obviously, this mechanism of the sub-bandgap absorption cannot be used to explain the visible absorption dependent on the metal electrode.

Fig. 5 shows the EQE (external quantum efficiency) of PZT film with metal Pt, Au, Cu and Ag top electrodes when PZT film is as-grown state (excluding the effect of remnant polarization). There is a strong peak at the wavelength of about 350 nm in every EQE curve, which is corresponding to the band-to-band absorption of PZT film. Obviously, the lower the work function of top metal electrode is, the stronger the peak becomes, which has been verified by other works that a low work function of metal electrode leads to a small Schottky barrier of top interface ($E_{bi\text{-}top}$) between PZT and metal electrode.[2] The EQE results of all structures are accordance with the results shown in Fig. 4. In the ITO/PZT/Pt and ITO/PZT/Cu structures, the photocurrent is close to zero at the visible band (400-750nm). In the ITO/PZT/Ag structure, the visible light with a shorter wavelength (400-550 nm) can lead to the photocurrent, which cannot be attributed obviously to the band-to-band absorption of PZT film. Similarly, the response at the visible band (500-700nm) in ITO/PZT/Au structure is not related to the band gap of PZT film.

To compare the measured photovoltaic enhancement and the SP properties of these structures, we reconstructed the PZT/metal electrode interface based on the AFM data of the polycrystalline PZT surface, and performed a finite element analysis of the optical properties of rough interface using the well-known commercial software Comsol Multiphysics. Fig. 6 shows the interface adopted in our simulations, of the size 1×1 μm, with the height distribution obtained by interpolating the AFM data (the actual 2-demetional AFM picture is shown here as a contrast, and the 3-demetional AFM picture can be seen in Supporting Information Fig. S4). The regions above and

below the interface are filled with PZT and electrode metals respectively, as shown in Fig. 6c. In the numerical simulations, the PZT/metal interface is illuminated from ITO electrode by a plane wave at normal incidence with a vacuum wavelength λ_0 ranging from 350nm to 750nm. The spectral response of the refractive index (n) and the extinction coefficient (k) of PZT film are measured by the method of spectroscopic ellipsometry, as shown in Supporting Information Fig. S5. The dispersion relations of metallic electrodes are calculated by using a conventional Drude model for SP materials.[39,44]

Fig. 7 gives the absorption spectra of PZT surface with the Ag, Au, Cu and Pt electrodes obtained in our numerical simulations, compared with the results when the interface between PZT and the electrodes is smooth purposely. It is shown that the roughness of the interface almost has no effect on the absorption of Pt electrode. On the contrary, the apparent absorption peaks around 520nm and 610nm are respectively observed for the Ag and Au electrodes with rough surface. A weaker absorption peak presents at about 600nm for the Cu electrodes compared with that of Au electrode. For all four electrodes, there are no any absorption enhancement in the visible band (400-750 nm) when the surface of PZT film is smoothed purposely.

Furthermore, a dramatic increase of electromagnetic field near the metal surface occurs around these absorption peaks. Fig. 8a-8c shows the calculated distributions of field enhancement factor $|E|^2/E_0^2$ just outside the rough surface of Ag, Au and Cu electrodes for incident wavelength at 520nm, 610nm and 600nm respectively. As contrasts, the results for smooth surfaces are illustrated in Fig. 8e-8g. It is clearly

shown that the near fields associated with the resonance peaks in the absorption spectra (Fig. 7) are strongly enhanced at rough surfaces. Both the field distributions and the absorption features verify the occurrence of SP resonances at the rough PZT/(Ag, Au, Cu) interface, particularly for the Ag electrode where the strongest resonance peak is observed and the surface field is enhanced up to nearly two orders of magnitude. The maximum surface field enhancement factor at the rough Ag surface is about 639.0. The resonance effects for the Au and Cu electrodes are weaker, with the maximum surface field enhancement factor obtained as 66.5 and 44.1 respectively. For platinum, no obvious near-field enhancement is observed for any incident wavelength except for a slight lightning-rod effect at several sharp tips of the rough surface (Fig. 8d).[45] It seems that scattering from the surface roughness has destroyed the weak SP effect in platinum, resulting in the disappearance of the absorption peak and the field concentration.

The above results from numerical simulations clearly show how the surface roughness of polycrystalline PZT film in our experiments couple the incident light with localized SPs of Ag, Au and Cu electrodes. Our calculation absorption spectra of PZT surface for the Ag, Au and Pt electrodes are used to explain well the photovoltaic performance of PZT film illuminated by the visible light with different wavelength. It is interesting to note that in our experiments the "good" electrodes (Ag or Au) for the EQE enhancement in the visible range are also those "good" for the excitation of surface plasmon resonances. Previous work[38] shows that Cu is easily to be oxidized at the interface where sufficient oxygen atoms are provided by PZT, which can seriously

destroy the excitation of its weak SP resonances due to roughness.

It should be mentioned that the actual EQE spectrum (400-750 nm) of PZT film with either Ag or Au electrode shows a blue shift, compared with that of the calculated absorption spectrum. Previous studies of Au particles embedded in PZT have shown that the positions of SP resonances are very sensitive to the refractive index of PZT just surrounding the metallic particles.[35,36] A change of the refractive index of surrounding PZT regions by 0.1 may result in a shift of the resonance peak by 10-20 nm.[36] The value of the refractive index of PZT adopted in the above simulations has been taken from the measured results for the whole PZT films, which is certainly larger than the actual PZT refractive index near the PZT/metal interface since this region usually contains more vacancies. Supporting Information Fig. S6 and Fig. S7 show the calculated blue shifts of the absorption peaks of Ag and Au electrode when the refractive index of PZT in simulations is decreased.

Note that SP-assisted photovoltaic effects in broad-gap semiconductors, such as dye-sensitized solar cells or photocatalysis system based on TiO_2 (the gap is about 3.2 eV),[46-48] are usually attributed to the charge transfer process at the semiconductor/metal surface. The observed photocurrent in the visible range was usually explained by that the plasmon-induced electrons in the metal are driven by the field of Schottky barrier at the metal/semiconductor interface to drift into the adjoining semiconductor. According to this mechanism, an increased photo current due to SP should be observed if the height of Schottky barrier is enhanced. Theoretically, the height of Schottky barrier at the PZT/metal interface is determined

by the difference of work function between PZT film and metal layer. In fact, the height of Schottky barrier is affected largely by the space charge at the interface, especially when the metal electrode is deposited at room temperature, which has been verified by many previous works.[22,49] Post-annealing can effectively enhance the height of Schottky barrier at PZT/metal interface.[22] In order to qualitatively check the influence of Schottky barrier height on the photocurrent due to the SP, we annealed the ITO/PZT/Ag structure at 500 ^{o}C in air for 10 min. Fig. 9 shows that the EQE at the wavelength of 350 nm, which corresponds to the band-to-band absorption of PZT film, decreases after the Ag electrode is annealed. It means the value of top Schottky barrier at the PZT/Ag interface increases. The bottom Schottky barrier height of ITO/PZT interface is reckoned usually as a constant, which is almost not influenced by the post annealing.[22,49] It is interesting that the EQE at the visible band (400-550 nm) decrease rapidly when the Ag dots were annealed at 500 ^{o}C for 10 min. Similar phenomenon can also be found in the ITO/PZT/Au structure (Supporting Information Fig. S8). Obviously, the increased Schottky barrier height of PZT/metal interface may impede the transport of electron-hole pairs due to SP, as illustrated and discussed in the Supporting Information Fig. S9. We suggest that the conventional charge-transfer mechanism cannot account for the SP-induced photocurrent in a PZT film although PZT is also reckoned as a semiconductor with a large band gap (about 3.6 eV). The photocurrents observed in the visible range in our ITO/PZT/metal structures are contributed from the light-induced electron-holes excited by the enhanced near-fields at the PZT surface rather than direct charge transfer from the metallic electrode,

which has been verified in our numeric simulations. Our model can also be used to explain well the low value of the EQE at the visible band at the ITO/PZT/Ag or ITO/PZT/Au structure.

4. Conclusions

In summary, SPs were introduced successfully into the inartificial surface of PZT film by deposited top Ag and Au electrodes without complex technique and high cost, which can greatly increase the photovoltaic of PZT film deposited on ITO/quartz substrate by enhancing the visible light absorption due to SPs. The results from numerical simulations clearly show the surface roughness of polycrystalline PZT film in our experiments can couple the visible incident light with localized SPs of Ag and Au electrodes. The experimental results shows the Schottky barrier of PZT/metal interface impedes the transport of visible light-induced charges due to SPs when the photocurrent majorly determined by the bottom Schottky barrier of ITO/PZT interface. This work clarifies the issue that the light-induced charges due to SPs in semiconductor with a large band gap occur at the surface of the semiconductor other than that of the metal materials, and points out a new method to improve the photoelectric transformation efficient of solar cells based on the ferroelectric films.

Acknowledgements

We greatly appreciate the support in numerical simulations by Prof. Y Lai. This work supported by National Natural Science Foundation of China (Grant No. 51272166, 11274045, 51002022, 91233109), Hong Kong Polytechnic University Internal Grant (A-PL50) and a Project Funded by the Priority Academic Program Development of

Jiangsu Higher Education Institutions (PAPD).

Author contributions

F.G.Z. designed the experiments and wrote the manuscript. P.Z., X.F.W. and M.R.S. designed and performed the sample growth. J.X.Z. performed and analyzed the microstructures of the sample. W.D. and L.F. performed and analyzed the results on the ferroelectric and photovoltaic. Y.B.B. and X.Q.S. performed and analyzed the results of refractive index and extinction coefficient. W.H. and J.H.H. analyzed the band structure of all samples. H.S. designed and performed the analogous calculations. All authors contributed to the scientific discussion and edited the manuscript.

Notes and references

1 D. Daranciang, M. J. Highland, H. D. Wen, S. M. Young, N. C. Brandt, H. Y. Hwang, M. Vattilana, M. Nicoul, F. Quirin, J. Goodfellow, T. T. Qi, I. Grinberg, D. M. Fritz, M. Cammarata, D. L. Zhu, H. T. Lemke, D. A. Walko, E. M. Dufresne, Y. L. Li, J. Larsson, D. A. Reis, T. K. Sokolowski, K. A. Nelson, A. M. Rappe, P. H. Fuoss, G. B. Stephenson and A. M. Lindenberg, *Phys. Rew. Lett.,* 2012, **108**, 087601.

2 V. N. Harshan and S. Kotru, *Appl. Phys. Lett.,* 2012, **100**, 173901.

3 L. A. Delimova and V. S. Yuferev, *J. Appl. Phys.,* 2010, **108**, 084110.

4 M. Qin, K. Yao and Y. C. Liang, *Appl. Phys. Lett.,* 2009, **95**, 022912.

5 F. G. Zheng, J. Xu, L. Fang, M. R. Shen and X. L. Wu, *Appl. Phys. Lett.,* 2008, **93**, 172101.

6 L. Pintilie, I. Vrejoiu, D. Hesse, G. L. Rhun and M. Alexe, *Phys. Rev. B,* 2007, **75**,

104103.

7 F. Yan, G. N. Chen, L. Lu and J. E. Spanier, *ACS Nano,* 2012, **6**, 2353.

8 H. T. Yi, T. Choi, S. G. Choi, Y. S. Oh and S. W. Cheong, *Adv. Mater.,* 2011, **23**, 3403.

9 J. Seidel, D. Y. Fu, S. Y. Yang, L. E. Alarcon, J. Q. Wu, R. Ramesh and J. W. Ager, *Phys. Rew. Lett.,* 2011, **107**, 126805.

10 R. K. Katiyar, A. Kumar, G. Morell, J. F. Scott and R. S. Katiyar, *Appl. Phys. Lett*., 2011, **99**, 092906.

11 B. Chen, M. Li, Y. W. Liu, Z. H. Zuo, F. Zhuge, Q. F. Zhan and R. W. Li, *Nanotechnology,* 2011, **22**, 195201.

12 W. Ji, K. Yao and Y. C. Liang, *Adv. Mater.,* 2010, **22**, 1763.

13 T. Choi, S. Lee, Y. J. Choi, V. Kiryukhin and S. W. Cheong, *Science*, 2009, **324**, 63.

14 D. W. Cao, H. Zhang, J. Xu; L. Fang; W. Dong, F. G. Zheng and M. R. Shen, *Mater. Chem. and Phys.,* 2011, **129**, 783.

15 D. W. Cao, J. Xu, L. Fang, W. Dong, F. G. Zheng and M. R. Shen, *Appl. Phys. Lett.,* 2010, **96**, 192101.

16 R. Nechache, C. Harnagea, S. Licoccia, E. Traversa, A. Ruediger, A. Pignolet and F. Rosei, *Appl. Phys. Lett.,* 2011, **98**, 202902.

17 S. Y. Yang, L. W. Martin, S. J. Byrnes, T. E. Conry, S. R. Basu, D. Paran, L. Reichertz, J. Ihlefeld, C. Adamo, A. Melville, Y. H. Chu, C. H. Yang, J. L. Musfeldt, D. G. Schlom, J. W. Ager and R. Ramesh, *Appl. Phys. Lett.,* 2009, **95**, 062909.

18 M. Qin, K. Yao and Y. C. Liang, *Appl. Phys. Lett.,* 2008, **93**, 122904.

19 L. Pintilie, I. Vrejoiu, G. L. Rhun and M. Alexe, *J. Appl. Phys*., 2007, **101**, 064109.

20 S. R. Basu, L. W. Martin, Y. H. Chu, M. Gajek, R. Ramesh, R. C. Rai, X. Xu and J. L. Musfeldt, *Appl. Phys. Lett.,* 2008, **92**, 091905.

21 J. Shi, M. B. Starr and X. D. Wang, *Adv. Mater.,* 2012, **24**, 4683.

22 D. W. Cao, H. Zhang, L. Fang, W. Dong, F. G. Zheng and M. R. Shen, *Appl. Phys. Lett.,* 2010, **97**, 102104.

23 M. Ichiki, H. Furue, T. Kobayashi, R. Maeda, Y. Morikawa, T. Nakada and K. Nonaka, *Appl. Phys. Lett.,* 2005, **87**, 222903.

24 S. Y. Yang, J. Seidel, S. J. Byrnes, P. Shafer, C. H. Yang, M. D. Rossell, P. Yu, Y. H. Chu, J. F. Scott, J. W. Ager, L. W. Martin and R. Ramesh, *Nature Nanotech.,* 2010, **5**, 143.

25 Z. J. Yue, K. Zhao, S. Q. Zhao, Z. Q. Lu, X. M. Li, H. Ni and A. J. Wang, *J. Phys. D,* 2010, **43**, 015104.

26 G. L. Yuan and J. L. Wang, *Appl. Phys. Lett*., 2009, **95**, 252904.

27 J. Xu, D. W. Cao, L. Fang, F. G. Zheng, M. R. Shen and X. L. Wu, *J. Appl. Phys.,* 2009, **106**, 113705.

28 D. W. Cao, C. Y. Wang, F. G. Zheng, L. Fang, W. Dong and M. R. Shen, *J. Mater. Chem.,* 2012, **22**, 12592.

29 D. W. Cao, C. Y. Wang, F. G. Zheng, W. Dong, L. Fang and M. R. Shen, *Nano Lett.,* 2012, **12**, 2803.

30 X. L. Yang, X. D. Su, M. R. Shen, F. G. Zheng, Y. Xin, L. Zhang, M. C. Hua, Y. J. Chen and V. G. Harris, *Adv. Mater.,* 2012, **24**,1202.

31 J. J. Zhang, X. D. Su, M. R. Shen, Z. H. Dai, L. J. Zhang, X. Y. He, W. X. Cheng, M. Y. Cao and G. F. Zou, *Sci. Reports,* 2013, **3**, 2109.

32 W. L. Barnes, A. Dereux and T. W. Ebbesen, *Nature,* 2003, **424**, 824.

33 A. A. Harry and P. Albert, *Nature Mater.,* 2010, **9**, 205.

34 K. R. Catchpole and A. Polman, *Opt. Exp.,* 2008, **16**, 21793.

35 H. L. Chen, K. C. Hsieh, C. H. Lin and S. H. Chen, *Nanotechnology,* 2008, **19**, 435304.

36 K. C. Hsieh, H. L. Chen, D. H. Wan and J. Shieh, *J. Phys. Chem. C,* 2008, **112**, 11673.

37 G. H. Chan, J. Zhao, E. M. Hicks, G. C. Schatz and P. V. D. Richard, *Nano Lett.,* 2007, **7**, 1947.

38 P. R. Katherine, J. W. J. Edwin, P. S. Mark and E. S. Aaron, *J. Phys. Chem. C*, 2011, **115**, 1793.

39 S. Dror and C. William, *Modern introduction to surface plasmons*, Cambridge, UK: Cambridge University Press, 2010.

40 C. H. Seager, D. C. McIntyre, W. L. Warren and B. A. Tuttle, *Appl. Phys. Lett.,* 1996, **68**, 2660.

41 H. M. Chen and J. Y. Lee, *Appl. Phys. Lett.,* 1998, **73**, 309.

42 P. Zhang, D. W. Cao, C. Y. Wang, M. R. Shen, X. D. Su, L. Fang, W. Dong and F. G. Zheng, *Mater. Chem. and Phys.,* 2012, **135**, 304.

43 R. Takahashi, T. Tybell and M. Lippmaa, *J. Appl. Phys.,* 2012, **112**, 014111.

44 A. D. Rakic, A. B. Djurisic, J. M. Elazar and M. L. Majewski, *Appl. Opt.,* 1998, **37**,

5271.

45 J. A. Schuller, E. S. Barnard, W. S. Cai, Y. C. Jun, J. S. White, M. L. Brongersma, *Nat. Mater.,* 2010, **9**, 193.

46 Z. W. Seh, S. H. Liu, M. Low, S. Y. Zhang, Z. L. Liu, A. Mlayah and M. Y. Han, *Adv. Mater.,* 2012, **24**, 2310.

47 E. S. Mohammed, E. S. Martha, H. Salah, P. Nicole, L. Abdelilah, D. Matthias and C. H. Solterbeck, *Adv. Funct. Mater.,* 2010, **20**, 377.

48 Z. H. Zhang, L. B. Zhang, M. N. Hedhili, H. N. Zhang and P. Wang, *Nano Lett.,* 2013, **13**, 14.

49 R. Schafranek, S. Payan, M. Maglione and A. Klein, *Phys. Rev. B* **2008**, *77*, 195310.

Figure captions

Figure 1. Illustration of the separation of photoinduced electrons and holes in ITO/PZT/metal structure. (a) h_{BB} and e_{BB} are the UV light-induced charges due to the band-to-band absorption of PZT film. (b) Top Schottky barriers height was reduced greatly due to low work function of top electrode that is a good material for SP applications in the visible range. The visible-light induced charges (h_{SP} and e_{SP}) can also be separated by the bottom Schottky barrier.

Figure 2. Polarization hysteresis loops of ITO/PZT/Pt, ITO/PZT/Au, ITO/PZT/Cu and ITO/PZT/Ag structures. The inset in Figure 2 is the sketch map of all structures.

Figure 3. Photovoltaic current voltage (PVIV) curves of ITO/PZT/Pt, ITO/PZT/Au, ITO/PZT/Cu and ITO/PZT/Ag structures illuminated under a simulated sunlight (100 mW/cm^2, AM1.5G) when PZT film was in remnant polarization-up states (depolarization field directed to bottom ITO electrode).

Figure 4. Time-dependent short-circuit photocurrent (J_{SC}) of (a) ITO/PZT/Pt, (b) ITO/PZT/Au, (c) ITO/PZT/Cu and (d) ITO/PZT/Ag structures illuminated under the lights with different wavelength, which were realized by using the filters K9 (green line), JB420 (blue line) and CB550 (red line). Comparatively, the J_{SC} of all structures illuminated under a simulated sunlight (100 mW/cm^2, AM1.5G) were also shown here

(black line).

Figure 5. External quantum efficient (EQE) of ITO/PZT/Pt (black), ITO/PZT/Au (red), ITO/PZT/Cu (green) and ITO/PZT/Ag (blue) structures illuminated under the monochromatic light with the wavelength from 300 nm to 750 nm when PZT film was in polarization-up state.

Figure 6. Height distribution (a) of the interface in the simulations from the AFM data (b) of the polycrystalline PZT film. (c) Rough PZT/metal interface adopted in simulations. The scales of x, y and z axes are 1μm, 1μm and 50 nm, respectively.

Figure 7. Calculated absorption spectra of PZT surface with the Ag (black, left), Au (red, left), Cu (red, right) and Pt (black, right) electrodes. Solid：rough surface；Hollow：smooth surface.

Figure 8. Calculated distributions of field enhancement factor $|E|^2/E_0^2$ just above the surface of metallic electrodes. (a) and (e) Ag electrodes for the incident light with a wavelength 520 nm for rough and smooth surface, respectively; (b) and (f) Au electrodes for that 610 nm; (c) and (g) Cu electrodes for that 600 nm; (d) and (h) Pt electrodes for that 600 nm.

Figure 9. External quantum efficient (EQE) of ITO/PZT/Ag structures illuminated under the light with the wavelength between 300 nm and 750 nm when PZT film was in polarization-up state. Blue line shows the EQE of ITO/PZT/Ag structure (Ag dots were unannealed), which is the same as that in Figure 5. Wine line represents that of ITO/PZT/Ag structure, where Ag dots were annealed at 500 ^{o}C for 10 min.

Figure 1

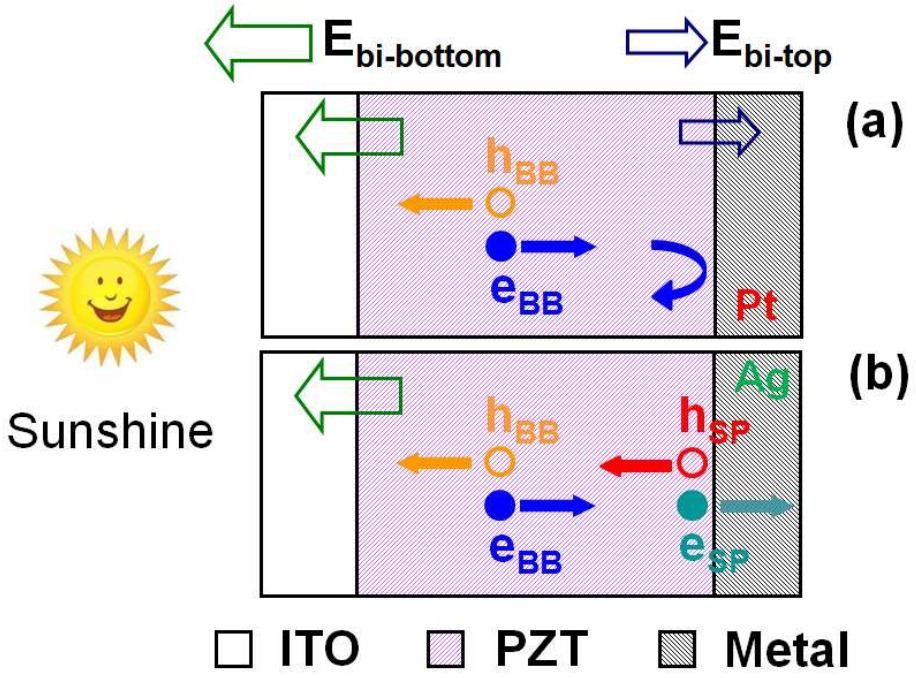

Figure 2

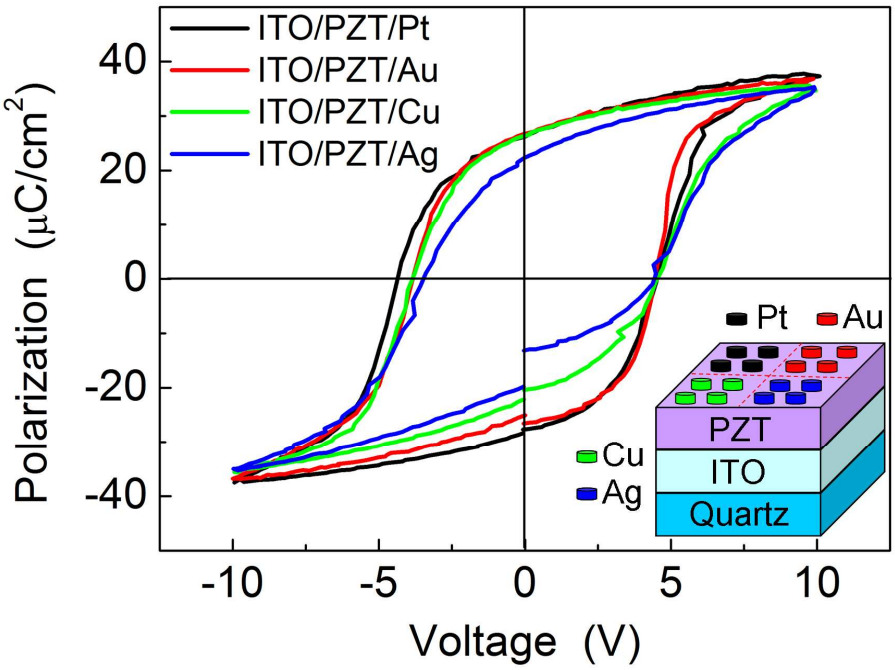

Figure 3

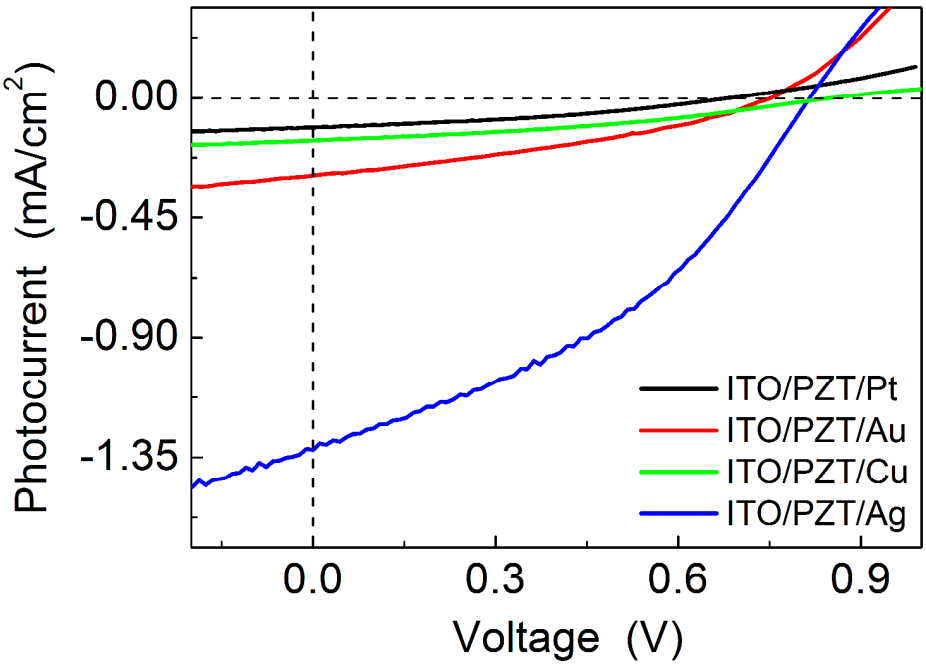

Figure 4

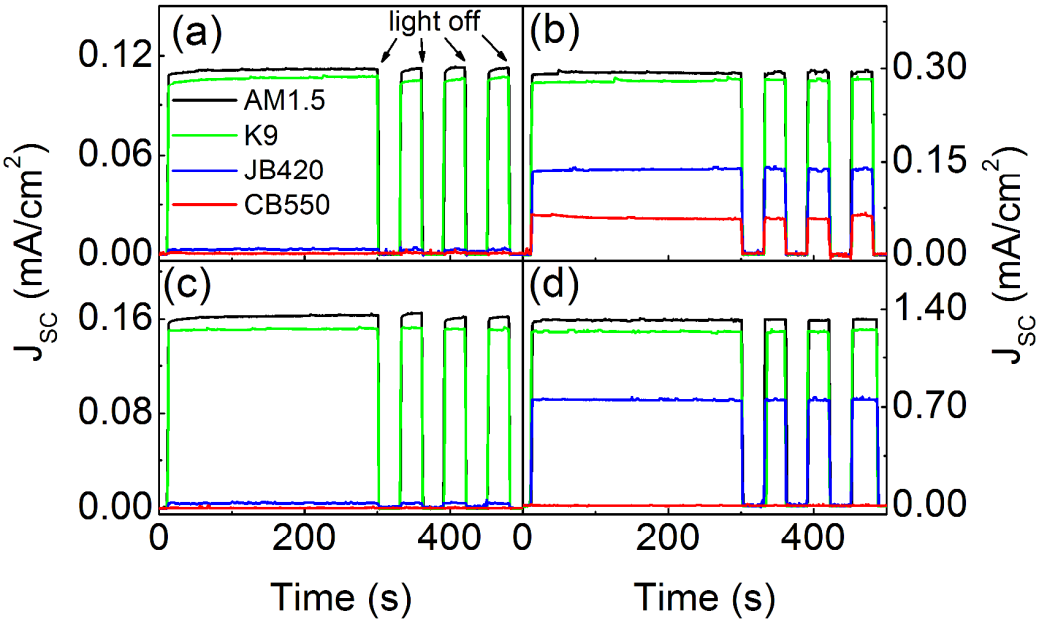

Figure 5

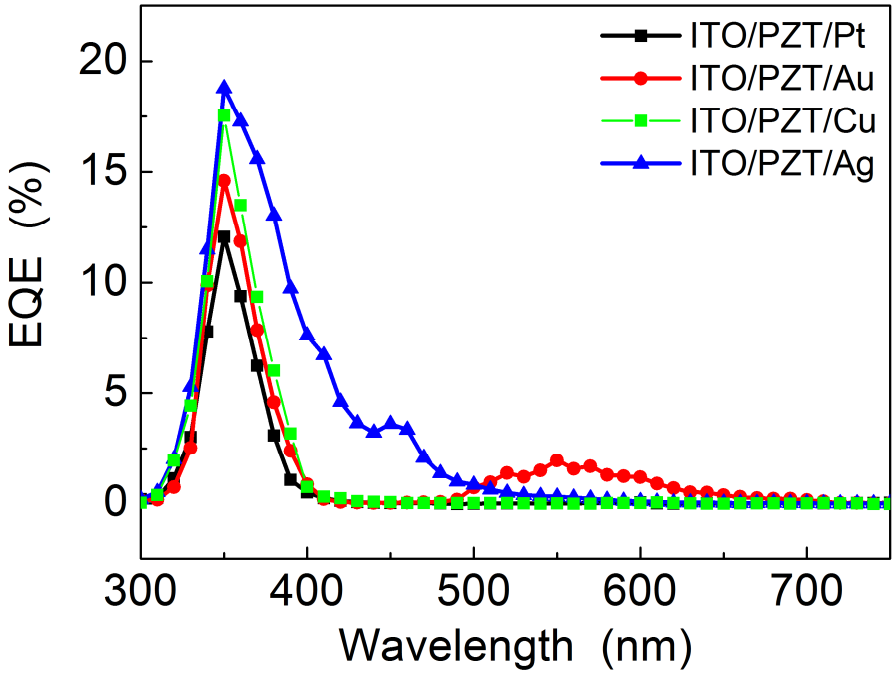

Figure 6

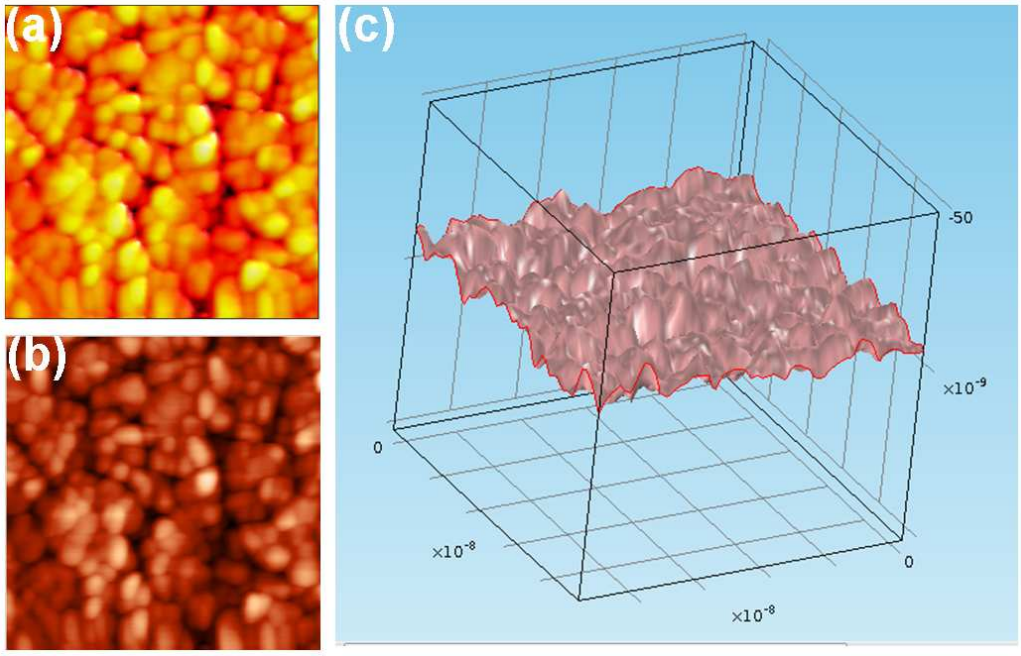

Figure 7

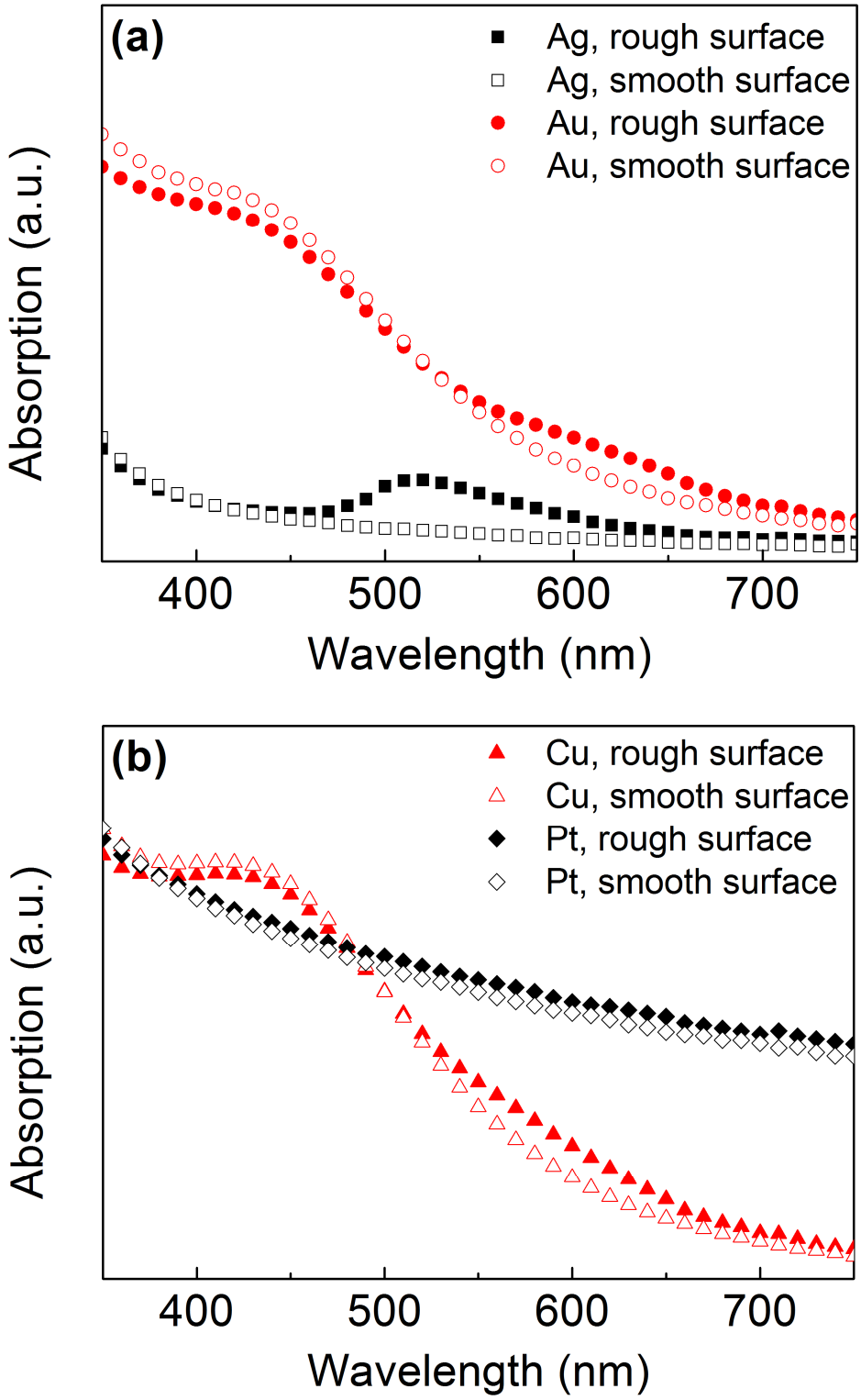

Figure 8

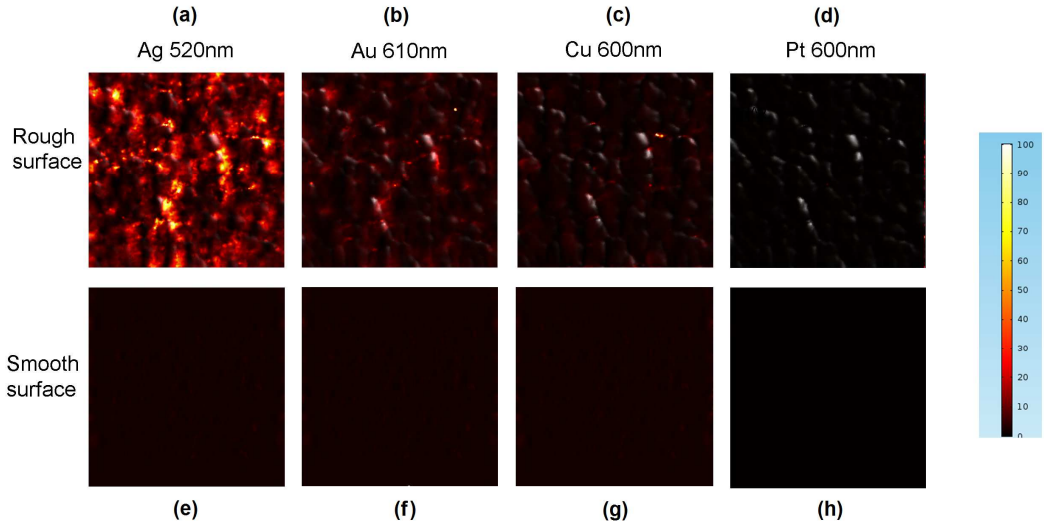

Figure 9